Frank, U., Nowaczyk, N., Frederichs, T., Korte, M. (2017): Paleo- and rock magnetic investigations on Late Quaternary sediments from low latitudes I: Geomagnetic paleosecular variation and relative paleointensity records from the Tobago Basin, Southeast Caribbean. - *Geophysical Journal International*, *208*, 3, pp. 1740—1755.

DOI: http://doi.org/10.1093/gji/ggw481

Geophysical Journal International

Geophys. J. Int. (2017) **208,** 1740–1755
Advance Access publication 2016 December 23
GJI Geomagnetism, rock magnetism and palaeomagnetism

doi: 10.1093/gji/ggw481

Palaeo- and rock magnetic investigations on Late Quaternary sediments from low latitudes. I: geomagnetic palaeosecular variation and relative palaeointensity records from the Tobago Basin, Southeast Caribbean

Ute Frank,[1] Norbert R. Nowaczyk,[1] Thomas Frederichs[2] and Monika Korte[1]

[1]*GFZ German Research Centre for Geosciences, Telegrafenberg, D-*14473 *Potsdam, Germany. E-mail: ufrank@gfz-potsdam.de*
[2]*University of Bremen, Faculty 5 Geosciences, Klagenfurter Strasse, D-*28359 *Bremen, Germany*

Accepted 2016 December 21. Received 2016 December 20; in original form 2016 June 22

SUMMARY

Detailed palaeo- and rock magnetic investigations were carried out on two sediment cores from the Tobago Basin, Eastern Caribbean. The 2.8 m long profiles span the last 15 kyr, according to accelerator mass spectrometry ^{14}C dates. Global climatic variations marking the transition from the Pleistocene into the Holocene are clearly reflected in the rock magnetic parameters. Their variations reflect the contribution of the coarse-grained fraction to the bulk composition. However, fine-grained Ti-magnetite particles carry a fairly stable magnetization in sediments deposited in the last 10 kyr. Comparison of stacked directional records of characteristic remanent magnetization inclination and declination, with data obtained from geomagnetic field models revealed distinct similarities for most intervals and add to the knowledge about the variability of the geomagnetic field in this area poorly covered by experimental data. A stacked record of relative palaeointensity was also established, using anhysteretic remanent magnetization as normalization parameter. Thus, the intensity of the geomagnetic field was steadily decreasing in the Caribbean between 9 and 0 ka, a trend that does not fit to relative paleointensity records available from Northern Hemisphere stacks but matches other low-latitude records and the South Atlantic Palaeointensity Stack.

Key words: Palaeointensity; Palaeomagnetic secular variation; South America.

INTRODUCTION

During the last few decades, records of geomagnetic palaeosecular variations, directions and/or intensity, have been reconstructed from a wide variety of sediments and time intervals, such as collected, for example, in the GEOMAGIA database (http://geomagia.gfz-potsdam.de/, last accessed 11 January 2017, see references therein). High-resolution records for the last several thousand years were mostly obtained from lake sediments, whereas marine, loess and other terrestrial sediments are the main recorders of long-term variations over millions of years (Opdyke & Channell 1996). Together with archaeomagnetic and volcanic data, sediment records provide the basis for a set of global geomagnetic field models (Korte *et al*. 2009, 2011; Nilsson *et al*. 2014) aiming to better understand the evolution of the Earth's magnetic field and the underlying processes in its core. The validity of these models is limited by the availability of data, especially by sparse data coverage across low latitudes and the southern hemisphere (Korte *et al*. 2011). Thus, a set of sediment cores from low-latitude sites were selected for investigation within the scope of the project 'Evolution of the geomagnetic dipole moment and the South Atlantic Anomaly' funded by the PLANETMAG priority programme of the German Research Foundation (http://www.planetmag.de/, last accessed 11 January 2017). This project aims to provide new data sets for the Holocene, and thus better constraints to test the hypothesis that the South Atlantic Anomaly (SAA) is a recurring feature. Cores from both sides of the Atlantic were selected for this study on the basis of the information given in cruise reports, publications and, in case of cores from the Ocean Drilling Program (ODP), on the data available in the ODP database (http://www-odp.tamu.edu/database, last accessed 11 January 2017). Here, we present the first results of this ongoing study obtained from two sediment cores from the Caribbean.

Site location and material

Cores M35003-4 (12°5.4′N, 61°14.6′W, 1299 m water depth) and M78/1_235-1 (11°36.5′N, 60°57.9′W, 852 m water depth) were taken in the Tobago Basin, southeast of Grenada during RV Meteor cruises 35 (Hemleben *et al*. 1998) and 78 (Schönfeld *et al*. 2011), respectively (Fig. 1). The Tobago Basin, a forearc basin of the Barbados accretionary prism, is part of the Eastern Antilles' eastern margin and is situated in front of the Lesser Antilles

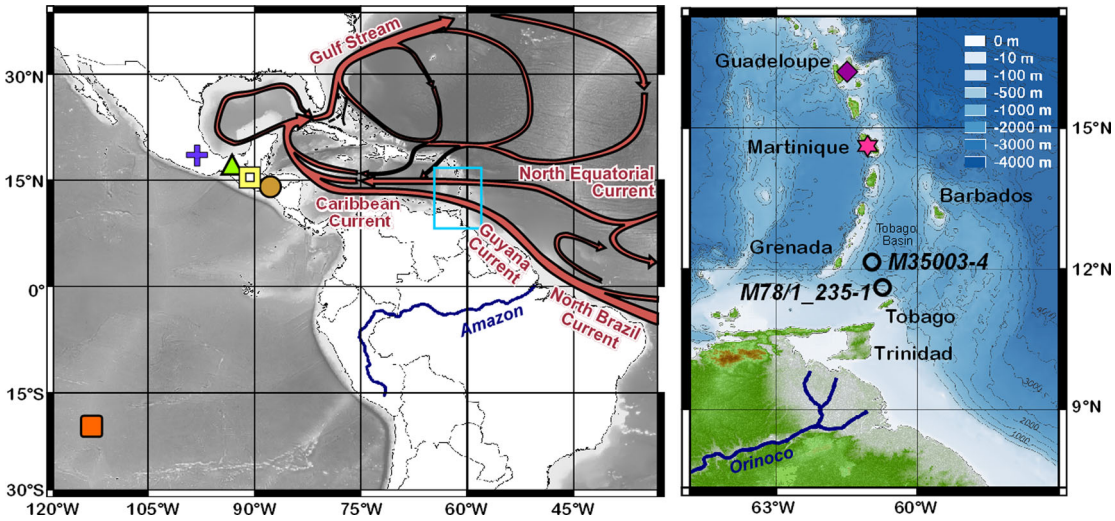

Figure 1. Left: overview of the main ocean current systems of the Caribbean and the north of South America, and right: geographical position of core locations within the Lesser Antilles island arc on a bathymetric map. Locations referred in the text are marked by coloured symbols. Orange filled square: East Pacific Rise; blue cross: Transmexican Volcanic Belt; green triangle: Chiapas, Mexico; yellow open square: Guatemala; golden filled circle: El Salvador; pink star: Montagne Pelee, Martinique and purple diamond: Basse Terre, Guadeloupe.

volcanic arc (Bouysse & Mascle 1994). Surface circulation and hydrography in this area are defined by the Guyana current as part of the South Equatorial current system (Fig. 1), transporting riverine material from the Amazon and Orinoco outflows northwestwardly along the Brazilian shelf through straits between the Lesser Antilles into the Caribbean Sea (Johns *et al*. 2002). The material transported through the Grenada passage and the Gulf of Paria (Fig. 1) is mainly derived from the Orinoco River (Bahr *et al*. 2013), whereas most of the discharge from the Amazon River is found to enter into the Caribbean Sea north of 14°N (Chérubin & Richardson 2007). Piston cores M35003-4 and M78/1_235-1 are of 9.63 and 12.30 m length, respectively, and consist of homogeneous olive-grey sediments, described as carbonate-rich silty clays (Vink *et al*. 2001; Schönfeld *et al*. 2011). Core M35003-4 has a mean $CaCO_3$ content of 10 wt% (Hüls 1999) and a total organic carbon (TOC) content between 0.2 and 0.9 wt% (Vink *et al*. 2001). Although the sediments of both cores look similar by eye, it can be assumed, that the sediment composition in these cores differ slightly, since the core locations are situated 60 km apart, with M350003-4 closer to the volcanic isle of Grenada (Fig. 1).

METHODS

Subsampling and magnetic investigations

The uppermost 286 cm of core M35003-4 and 285 cm of core M78/1_235-1 were subsampled with rectangular plastic boxes (20 × 20 × 15 mm) pushed into the surface of the split core sections in intervals of 20 mm. A filled sample was removed before the next box was pressed into the sediment in order to obtain the highest resolution possible in cores that were already subsampled for other scientific investigations. Thus, a total of 252 samples was obtained and all samples were subjected to a standardized set of palaeo- and rock magnetic measurements, including low-field magnetic susceptibility measurements (κ_{LF}) alternating field (AF) demagnetization of the natural remanent magnetization (NRM), imprint and AF-demagnetization of an anhysteretic remanent magnetization (ARM), imprint of a saturation isothermal remanent magnetization (SIRM) and others, as listed in more detail in Table 1. An alternating gradient magnetometer 'MicroMag' was used in order to obtain complete IRM acquisition curves and hysteresis parameters from 12 samples from each core representing the various lithologies within each core. Out of these, a total of six samples were selected for temperature-dependent measurements of magnetic susceptibility with the Multifunction Kappabridge (MFK-1). In addition, all samples were weighted to get supplementary information on the sediment composition by means of wet bulk density. Stability of NRM was tested by stepwise AF demagnetization with the in-line three-axis AF demagnetizer in 10 steps to fields of up to 100 mT (Table 1 and Fig. 2). The directions of the characteristic remanent magnetization (ChRM) were calculated from the results of successive demagnetization steps (15–65 mT) by means of principle component analysis (Kirschvink 1980). Since the cores were obtained without absolute azimuthal orientation, the mean ChRM declination value was set to zero. The ChRM declination record of M78/1_235-1 was affected by a twisting of the core during recovery and the trend of 10° m^{-1} was corrected by a linear regression algorithm.

Magnetic extracts and scanning electron microscopy

Magnetic extracts were taken from two samples from core M35003-4 (43 and 264 cm depth) and three samples from core M78/1_235-1 (39, 95 and 141 cm depth). To obtain these extracts, 2 cm^3 of sediment from each sample was mixed with ethanol in a small glass bottle and thoroughly shaken. The magnetic minerals were then extracted from this slurry by a strong magnet held against the outside of the bottle. A pipette was used to collect the magnetic particles from the inner wall of the bottle and place them onto a glass slide. After evaporation of the ethanol, a standard scanning electron microscopy (SEM) stub, covered with a double-sided sticky tape, was pressed onto the dried extract. The samples were then sputtered with carbon. Analyses were performed with a Carl Zeiss SMT Ultra 55 Plus SEM with integrated energy dispersive X-ray spectrometry facility, which has a spatial resolution of 1 nm at 20 keV, following the procedure described by Nowaczyk (2011).

Table 1. Palaeo- and rock magnetic investigations carried out on all samples from sediment cores M35003-4 and M78/1_235-1, Tobago Basin.

Investigation	Instrument	Remarks
Measurement of low-field magnetic susceptibility (κ_{LF})	AGICO Kappabridge MFK-1A	Operating frequency 875 Hz
Measurement and subsequent demagnetization of natural remanent magnetization (NRM)	2G Enterprises cryogenic magnetometer (2G-755-SRM) including an in-line triaxial alternating field demagnetizer	11 steps up to 100 mT: 0, 5, 10, 15, 20, 30, 40, 50, 65, 80 and 100 mT
Imprint of anhysteretic remanent magnetization (ARM)	2G Enterprises 600 single-axis demagnetizer including an ARM-coil (max. static field 1 mT)	Produced along positive *z*-axis, static field: 0.05 mT, AF amplitude: 100 mT
Measurement and subsequent demagnetization of ARM	2G Enterprises cryogenic magnetometer (2G-755-SRM)	11 steps up to 100 mT, same as for the NRM
Imprint of saturation isothermal remanent magnetization (SIRM)	2G Enterprises 660 pulsemagnetiser (max. amplitude 2.7 T)	Produced along positive *z*-axis, peak field of 1.5 T, back field -0.2 T for *S*-ratio calculation
Measurement of SIRM	Molyneux Minispin Fluxgate magnetometer	

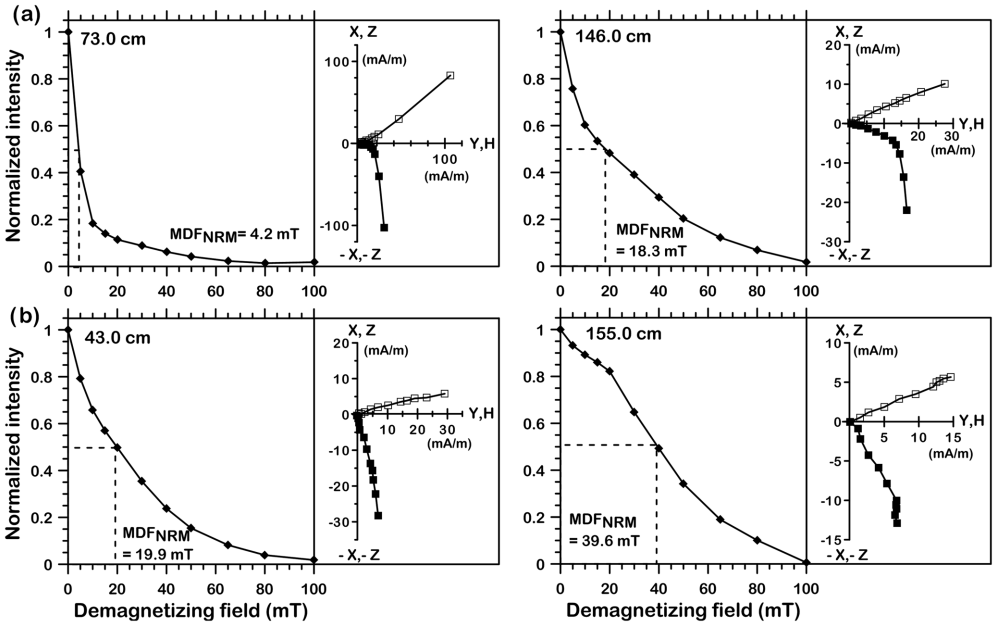

Figure 2. Results from alternating field demagnetization of the natural remanent magnetization (NRM) of two samples each from (a) core M35003-4 and (b) core M78/1_235-1. Sampling depth and median destructive field (MDF) of each sample are indicated. The corresponding orthogonal projections (vector endpoint diagrams) of components of the magnetization vectors during demagnetization in fields from 0 to 100 mT are shown additionally. Closed symbols denote X plotted versus Y (horizontal plane) and open symbols denote Z plotted versus H (vertical plane).

Correlation and chronology

The correlation between both cores is based on the results from rock magnetic measurements from the subsamples, complemented by the shipboard logs of magnetic susceptibility and colour reflectance. The colour data from core M35003-4 were digitized from the cruise report (Hemleben *et al*. 1998), whereas the data from core M78/1_235-1 are available from the PANGAEA database (Bahr 2012a,b). As can be seen from Fig. 3(a) a better match between both cores is given by parameter ratios, here J_{NRM} (NRM intensity) after demagnetization in a field of 20 mT (J_{NRM20}) divided by κ_{LF}, and not by the variations in concentration-dependent parameters (e.g. κ_{LF} in Fig. 3a). Between 184 and 221 cm depth in core M78/1_235-1, no sediment was available for subsampling, correlation is here solely based on shipboard data (Fig. 3a).

In order to obtain a consistent chronology for all records, the available accelerator mass spectrometry (AMS) ^{14}C ages from both cores were combined, using the correlation scheme presented in Fig. 3(a). For core M35003-4, a total of 19 AMS ^{14}C is available (Rühlemann *et al*. 1999; Hüls & Zahn 2000), with seven ages in the time interval investigated (Fig. 3b). Core M78/1_235-1 is dated by 4 AMS ^{14}C determinations interspersed throughout the uppermost 3 m of the sediments (Hoffmann *et al*. 2014a). All AMS ^{14}C ages are available from the PANGAEA database (https://www.pangaea.de/, last accessed 11 January 2017, Rühlemann *et al*. 2006; Hoffmann

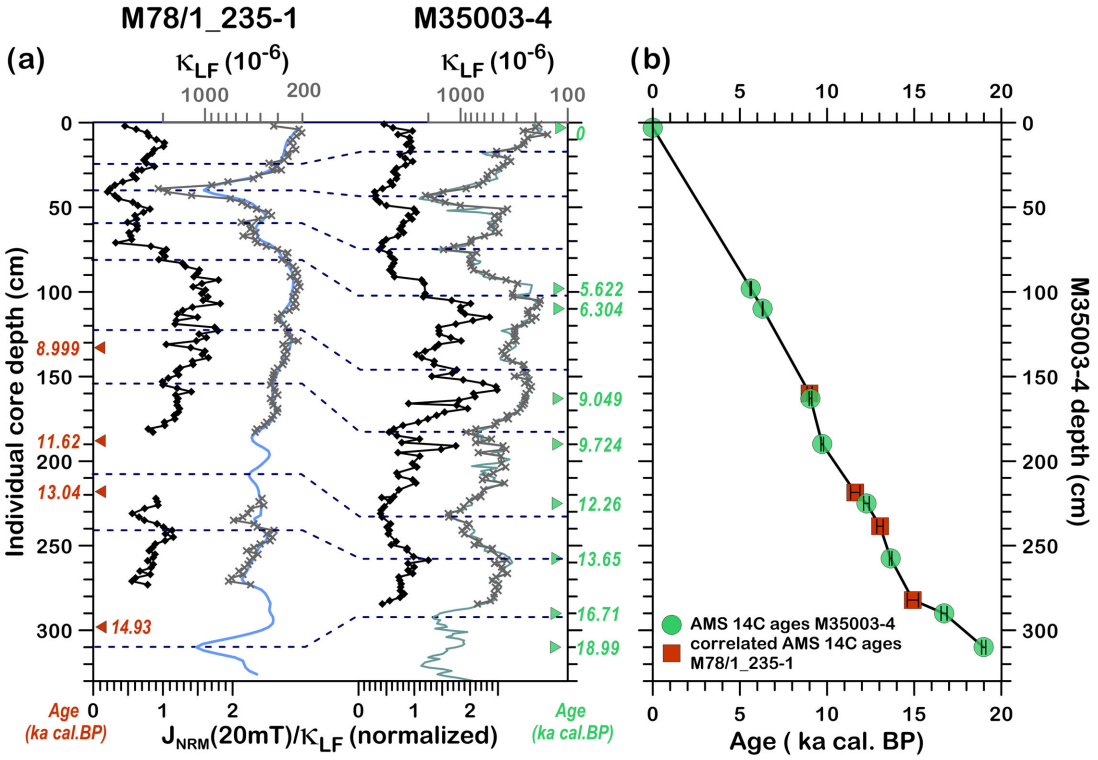

Figure 3. (a) Down-core plots of low-field magnetic susceptibility (κ_{LF}) of discrete samples and ratio of NRM intensities after demagnetization at 20 mT (J_{NRM20}) divided by κ_{LF} and then normalized to the mean value versus individual core depth. The blue and green lines show the continuous shipboard measurement of magnetic susceptibility of core M78/1_235-1 (Bahr 2012b) and M35003-4 (Hemleben *et al*. 1998), respectively. The dashed lines show correlation tie points in both cores. In addition, the positions of available calibrated AMS ^{14}C ages for both cores are shown. (b) Composite depth–age model for the cores from Tobago Basin. All error bars for the AMS ^{14}C ages are smaller than the size of the symbols.

et al. 2014b). In order to have the same calibration standard for both data sets, the AMS ^{14}C dates from core M35003-4 were re-calibrated using CALIB 7 (Stuiver & Reimer 1993; Stuiver *et al*. 2013) applying a reservoir correction of 400 yr as in the original calibration (Rühlemann *et al*. 1999; Hüls & Zahn 2000). Plotting all ages versus M35003-4-depth reveals a remarkably good agreement (Fig. 3b) between the cores. The depth–age transformation was done by linear interpolation between the given ages, yielding sedimentation rates between 17 and 40 cm kyr^{-1}, and an age of around 15 ka cal. BP for the oldest sediments investigated (Fig. 3b).

RESULTS AND DISCUSSION

Rock magnetism

Magnetite and Ti-magnetite were identified as the two dominant magnetic carrier minerals in the sediments from the Tobago Basin by their Curie temperature of 580 and ~280 °C, respectively, using high-temperature measurements of magnetic susceptibility (Fig. 4). In the samples from 43 cm (M35003-4) and 39 cm (M78/1_235-1) depth, taken from an interval that is marked by a distinct increase in concentration of magnetic minerals (Fig. 3a), a heterogeneous but similar composition for both cores is evident (Fig. 4), suggesting an identical source of the terrigenous material. Apart from that, there are notable differences between the records obtained from both cores: sediments from core M35003-4 exhibit a higher amount of magnetite, while samples from core M78/1_235-1 display a pronounced transformation of paramagnetic minerals into magnetite during the heating experiments (Fig. 4). These differences must be attributed to the different locations with respect to the flow direction of the Guyana current, the distance to the volcanic arc, and to the Orinoco river mouth, as well as to different water depths. All these factors are influencing the grain size and the percentage of the terrigenous component in the sediment. SEM analyses of magnetic extracts from both profiles confirm the presence of Ti-magnetite and magnetite (Figs 5a–c), with haematite (Fig. 5a), pyrite (not shown) and manganese- and/or chromium-bearing magnetite (Fig. 5d) as additional (magnetic) minerals with variable amounts in both cores. According to the *S*-ratio values, haematite plays only a minor role (Fig. 5a).

Hysteresis parameters of the Ti-magnetites plot in the pseudo-single domain (PSD) range, with less scatter for core M78/1_235-1 (Fig. 6). All samples follow the hyperbolic trend of the single domain (SD)—multidomain (MD)—mixing line based on data from Parry (1980, 1982), as presented in Dunlop (2002) and group slightly above the mixing curve for an MD contribution between 60 and 70 per cent (Fig. 6). The slight shift to higher B_{CR}/B_C-ratios here is probably due to the presence of haematite, which has a greater effect on the coercivity of remanence B_{CR} than on the coercivity B_C (Roberts *et al*. 1995; Frank & Nowaczyk 2008).

In Fig. 7, the rock magnetic results from both cores M35003-4 and M78/1_235-1 are shown versus age. Variations in magnetic concentration, grain size and coercivity for both cores are similar, suggesting a common sediment source, transport, depositional mechanism and postdepositional conditions. In general, intervals of higher concentration of magnetic grains (high values for κ_{LF}, J_{ARM} and J_{SIRM}) are characterized by larger magnetic grain sizes (low

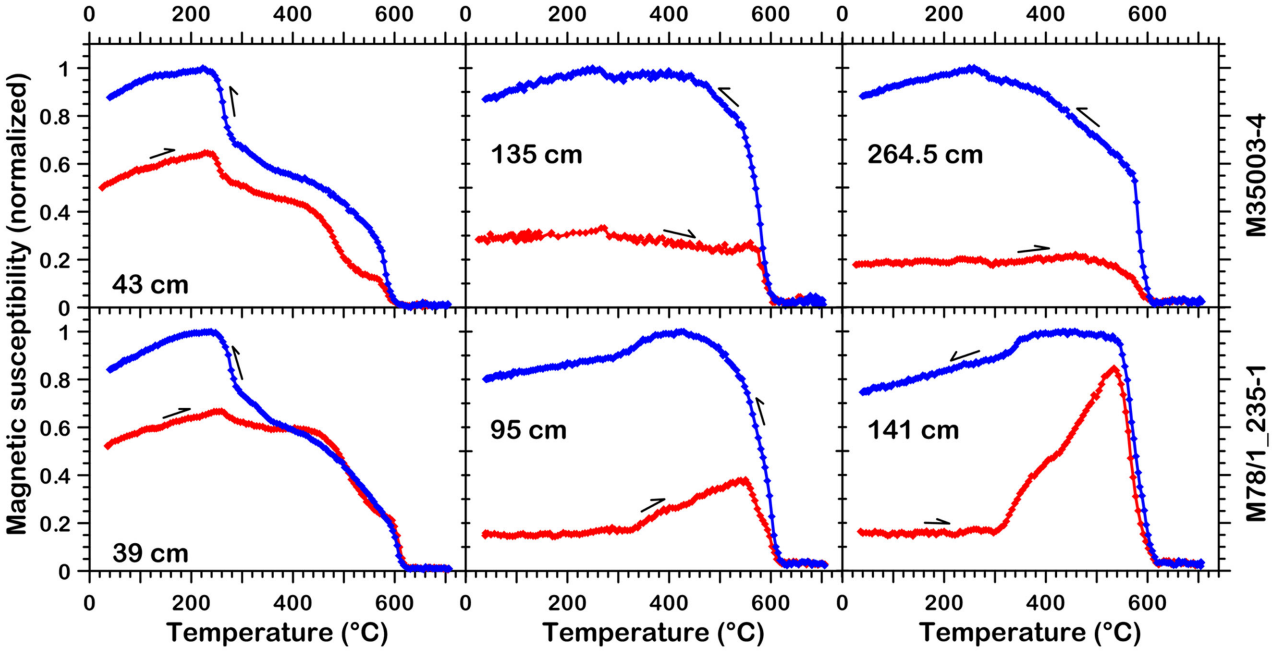

Figure 4. Temperature-dependent measurements of magnetic susceptibility from three samples each from core M35003-4 (top) and core M78/1_235-1 (bottom). Red lines denote heating and blue lines cooling curves.

values for κ_{ARM}/κ_{LF} and J_{ARM}/J_{SIRM}), indicating that coarser magnetic grains were deposited during intervals with increased influx of magnetic minerals (Fig. 7). The median destructive field of the ARM (MDF_{ARM}), reflecting the magnetic coercitivity, is also lower in intervals dominated by coarser magnetic grains. This is especially visible at around 4 and 2.5 ka (Fig. 7), when distinct peaks in concentration coincide with drops in coercitivity. Since this affects both cores similarly, it may result from changes in the sediment load of the Guyana current and thus changes in the outflow from the Orinoco and Amazon Rivers. However, throughout the whole time interval investigated, there is a distinctly higher amount of coarse-grained magnetic minerals in M35003-4, as reflected by twice as high J_{SIRM} values, and in consequence, in the ratio of J_{ARM}/J_{SIRM} (Fig. 7), as well as in lower MDF_{ARM} values. This is probably due to local conditions affecting the sediment load of the individual branches of the Guyana current in front of the windward islands of the Lesser Antilles (Fig. 1). There is no clear proof that terrigenous material from the volcanic arc itself contributes to the sediment compositions of cores M35003-4 and M78/1_235-1, but it cannot be ruled out either. The vast extent of the catchment areas of both the Amazon and the Orinoco River alone is sufficient to account for the observed variations in magnetic mineralogy.

In order to illustrate the climate-induced variability in magnetic concentration and grain size, the J_{SIRM} and the J_{ARM}/J_{SIRM} curves were compared to records reflecting variations in sediment composition, as obtained from different studies on core M35003-4 (Fig. 8; Rühlemann *et al*. 1999; Hüls & Zahn 2000; Vink *et al*. 2001). For example, variations in the rock magnetic parameters match those in the palaeoproductivity (Vink *et al*. 2001), the content of C^{37} alkenones (Rühlemann *et al*. 1999) and the content of terrigenous material (Vink *et al*. 2001), with lower magnetic concentrations and smaller grain sizes during intervals with higher contents of biogenic remnants (Fig. 8). The changes in the amount of nutrients transported into the Tobago Basin are due to climatically controlled variations in the wind-driven coastal upwelling north of Brazil, in the riverine nutrient supply from the Amazon and the Orinoco Rivers, as well as in water temperature (Vink *et al*. 2001). Between 15 and 11 ka, the termination of the last glacial period, the dilution of the marine $CaCO_3$ signal by the riverine material is far smaller, due to a distinct decrease in Orinoco and Amazon River discharge (Maslin & Burns 2000; Hoffmann *et al*. 2014a). In addition, the sediments from the Amazon River are transported through submarine channels to the abyssal plain in front, rather than to the continental margin to be redistributed by longshore currents (Damuth 1977). The early Holocene, the so-called 'Holocene thermal maximum' (Haug *et al*. 2001), is characterized by reduced variability in the amount of terrigenous material, by high productivity and low sand content in combination with low concentrations of fine-grained magnetic particles (Fig. 8). Between 7.5 and 8 ka, a clear increase in the amount of magnetic minerals and their grain sizes coincides with a decrease in biogenic productivity (Fig. 8). Sediments younger than 5.5 ka show a higher variability in all rock magnetic parameters with concentrations rising up to values 10 times higher than in the underlying sediments and with a distinct increase in the amount of coarse-grained magnetic minerals. Peaks in the sand curve are matching with intervals of coarsest magnetic minerals. This increase in the amount of fine sand and coarser magnetic grains is interpreted as an enhanced contribution from the Orinoco River, as was derived from an end-member unmixing model of terrigenous material in core GeoB3938-1, located south of Barbados (Fig. 1; Govin *et al*. 2014).

Directional variations

ChRM inclination and declination records from both cores are shown in Fig. 9, together with the maximum angular deviation (MAD) and κ_{ARM}/κ_{LF} as an indicator for grain size variations. The

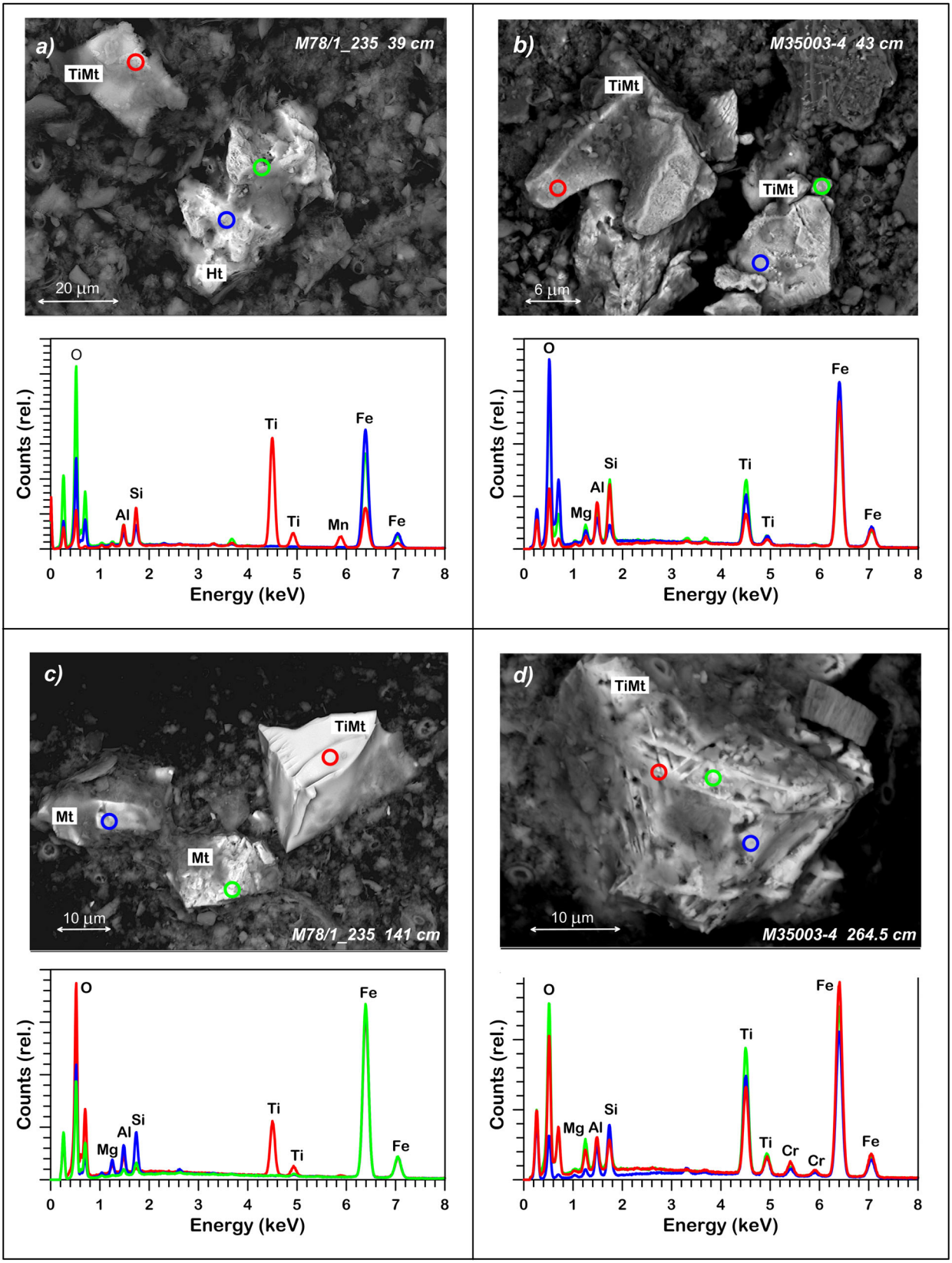

Figure 5. Magnetic mineral inventory of the sediments as derived from scanning electron microscopy (SEM) performed on magnetic extracts. (a) Irregular haematite and Ti-magnetite. (b) Various Ti-magnetites. (c) Magnetite and Ti-magnetite. (d) Residual Cr-rich Ti-magnetite with ilmenite lamellae. Spots for X-ray element analyses, shown below each photo, are indicated by corresponding coloured circles. For more details, see the text. SEM analyses were performed with a target distance of 11–13 mm, an aperture size of 120 µm, applying a voltage of 20 KV, using backscatter mode and Inlens detector, respectively. Ht = haematite, TiMt = Ti-magnetite and Mt = magnetite.

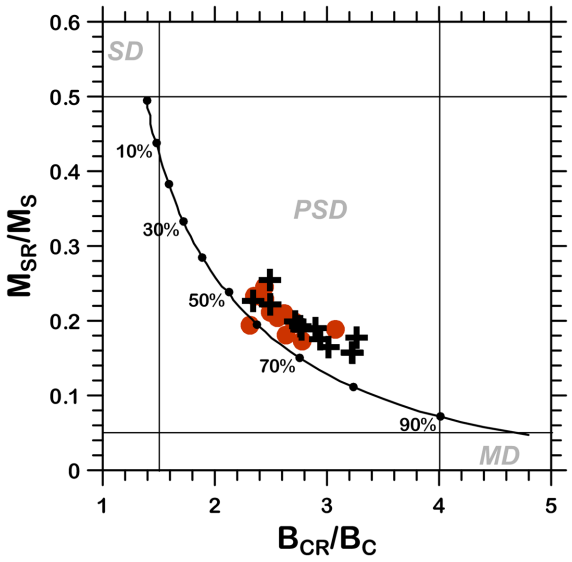

Figure 6. Results of hysteresis measurements carried out on 12 samples from core M35003-4 (black crosses) and 14 samples from core M78/1_235-1 (red filled circles) presented in a Day plot (Day *et al*. 1977). The SD-MD mixing line is curve 3 from Dunlop (2002).

variations in MAD clearly mirrors the variations in grain size, the remanence vectors are more stable (lower MAD) in intervals with finer grains (higher κ_{ARM}/κ_{LF}). Comparing the results from both cores, it could be assumed, that the quality of the data obtained from core M78/1_235-1 is better than that from core M35003-4, due to the generally lower percentage of coarse-grained Ti-magnetite in this core. But in the time interval from 1 to 5.5 ka, characterized by a distinct increase in concentration (Fig. 7) and the amount of coarse-grained magnetic minerals, generally higher MAD values were obtained in both cores (Fig. 9). This link between grain size of the magnetic mineral fraction and MAD is more pronounced in core M35003-4, resulting in a more scattered directional record, especially in the interval 9–14 ka.

The mean inclination of ChRM is 6° lower than the expected dipole inclination of 23.2° and 22.3° for cores M35003-4 and M78/1_235-1, respectively. The amplitudes of the variations in inclination and declination are in the range of ±20° which corresponds to typical lacustrine geomagnetic palaeosecular variation (PSV) records. Although high MAD values indicate that these sediments might not be ideal recorders of PSV, stacked inclination and declination records were created for the Tobago Basin by numerical resampling of the data sets from cores M35003-4 and M78/1_235-1 in 0.1 kyr steps and subsequent arithmetic calculation of mean values for each time slice (Fig. 10). There are less differences between both individual inclination records than between the declination records, with the latter showing opposite trends in the time interval 3.5–6 ka (Fig. 10). This interval is marked by a pronounced increase in magnetic concentration in core M35003-4 but not in core M78/1_235-1 (Fig. 7). The associated changes in magnetic grain size and in the MAD (Fig. 9), however, are similar in both cores, indicating that changes in the amount of magnetic minerals did not necessarily affect the stability of the remanence. Interestingly, the differences between the individual records are not necessarily linked to the MAD values. Neither are there bigger divergences between the curves in intervals where the MAD values of both cores are clearly different (9–14 ka), nor are high MAD values leading to an increase in divergence (2–6 ka, I_{CHRM}) (Fig. 10). However, in time intervals with a MAD < 4° in both cores, intervals where the finest magnetic grains were deposited (Figs 7 and 9), the agreement between inclination and declination records are decent. These observations indicate that there is only a minor influence of the grain size variations on the quality of the recorded directional signal in the sediments from cores M35003-4 and M78/1_235-1 and the lithology is not a direct control on the mean direction obtained by stacking the cores.

In the following figures, the error range, given by the differences between the individual records and the mean values, is marked as grey band. The stacked directional records were compared to records obtained from numerical models CALS10K.1b (Korte *et al*. 2011) and pfm9k.1a (Nilsson *et al*. 2014), as well as to data obtained from pyroclastic deposits from Montagne Pelée, Martinique (Genevey *et al*. 2002; Tanty *et al*. 2015), andesitic lava flows from Basse Terre, Guadeloupe (Carlut & Quidelleur 2000) and archaeomagnetic direction data from El Salvador (Eighmy & Sternberg 1990) (Fig. 11). Both islands, Martinique and Guadeloupe, are situated north of Tobago Basin at 14.8°N and 16°N, respectively (Fig. 1). AMS ^{14}C ages are shown in order to illustrate where the age models of cores M35003-4 and M78/1_235-1 have a lower coverage in terms of absolute dating. Between 0 and 5 ka, there are probably short-lived changes in sedimentation rate as suggested by peaks in concentration and grain size (Fig. 7), but this could not be resolved by the depth–age model. Thus, the inclination and declination records for this time interval probably must be slightly adjusted in order to fit to the archaeomagnetic data and palaeomagnetic data from volcanic material. There are distinct similarities between the modelled directional curves and the records obtained from Tobago Basin between 6 and 10 ka, being the interval with the most stable magnetization, especially in the declination record (Fig. 11). Model data fit better to the volcanic data, which was hitherto the only source of information in this region before, but there are some congruencies with the sediment record as well.

Knowing that they are located several 1000 km to the west (Hoya de San Nicolas, Mexico; Chaparro *et al*. 2008), northwest (Hall's Cave, Texas; Bourne *et al*. 2016) and north (Bermuda Rise; Lund & Keigwin 1994), the closest sedimentary PSV records available for comparison are shown together with the stacked record from the Caribbean in Fig. 12. The sedimentation rates of the individual records range between ~45 cm kyr^{-1} for Hoya San Nicolas and ~10 cm kyr^{-1} for the sediments from the Bermuda Rise, the latter described as a 'low-pass filtered record of true magnetic field variability' for the Holocene (Lund & Keigwin 1994). The long-term variations, in particular the inclination records, look quite similar with the inclination curve from Hall's Cave corresponding to the Bermuda Rise curve (Fig. 12). Both are showing an increase of 15° in inclination between 16 and 10 ka and a subsequent decrease. The pronounced low in inclination at around 2 ka is also recorded in the Caribbean record (Fig. 12). An additional inclination feature as marked by black arrows is documented in both, the Caribbean and the Mexican record. It is accompanied by a similar feature in the declination records (Fig. 12). A more detailed correlation of short-term variations in inclination and declination is possible, but not necessarily advisable due to the differences in data quality and temporal resolution of the presented records. Caution is required when interpreting the differences in age between the features that can be correlated in the Caribbean and the Mexican records in terms of a westward drift (Fig. 12). In the future, additional information will be available from ongoing investigations on sediment cores

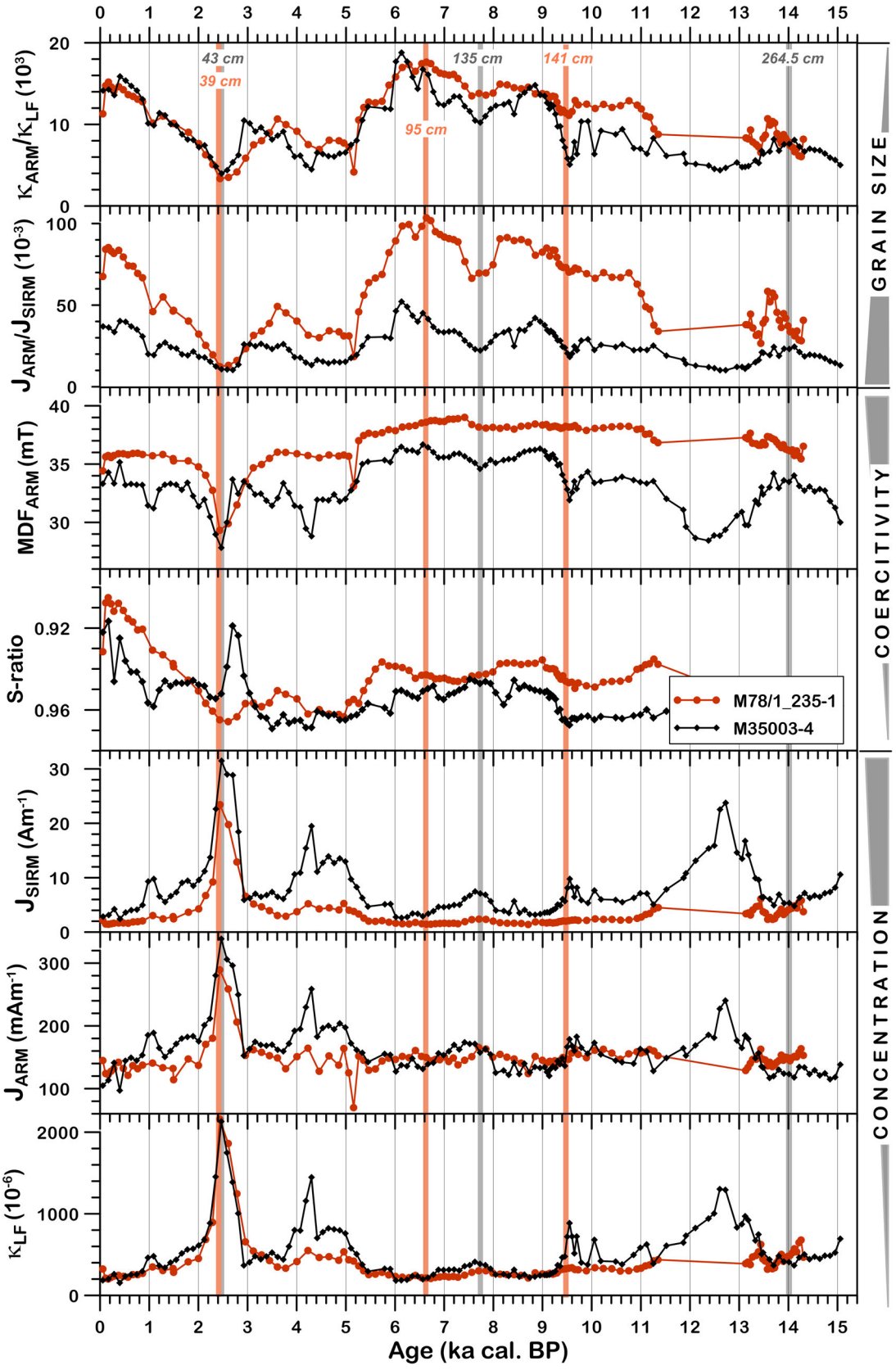

Figure 7. Time-series of the concentration-dependent parameters low-field magnetic susceptibility (κ_{LF}), intensity of anhysteretic remanent magnetization (J_{ARM}) and intensity of saturation isothermal remanent magnetization (J_{SIRM}) and records of parameters indicative of magnetic coercitivity and grain size: *S*-ratio, median destructive field of ARM (MDF_{ARM}), J_{ARM}/J_{SIRM} ratio and κ_{ARM}/κ_{LF} ratio, for cores M35003-4 and M78/1_235-1 versus age. *S*-ratio $= 0.5 \times (1 - IRM_{-0.2T}/SIRM_{1.5T})$. Vertical lines denote the positions of the samples shown in Figs 4 and 5. Light red lines: core M78/1_235-1 and grey lines: core M35003-4.

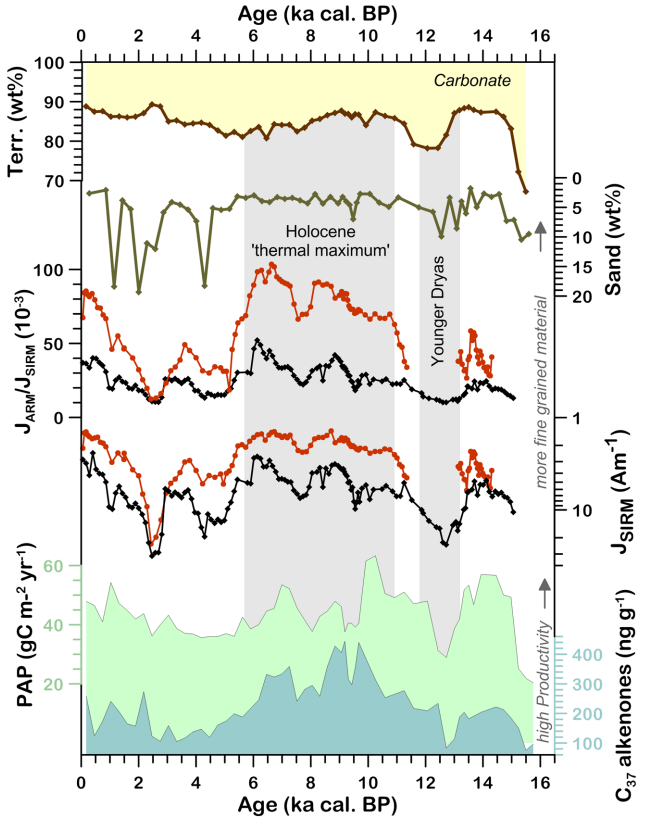

Figure 8. Magnetic concentration (J_{SIRM}) and grain size (J_{ARM}/J_{SIRM}) curves in comparison with records of climate-induced variability in sediment composition obtained from core M35003-4: palaeoproductivity PAP (blue) (Vink *et al*. 2001) and content of C37 alkenones (green) (Rühlemann *et al*. 1999) both reflecting biogenic productivity; percentage of terrigenous material (Vink *et al*. 2001) and percentage of sand fraction (Hüls & Zahn 2000). Black curves: M35003-4 and red curves: M78/1_235-1. The J_{SIRM} curves are plotted on a reverse scale.

from the North Brazilian continental slope (Roud 2014; Just private communication, 2015) providing further PSV time-series.

Relative palaeointensity estimation

There is no evidence for a relevant secondary magnetization carried by the magnetic mineral fraction in the sediments from Tobago Basin. Moreover, the constitutent magnetominerals exhibit a homogeneous composition with regard to mineralogy and concentration with the latter varying by less than a factor of five (Fig. 7) and therefore meeting the criteria by Schwartz *et al*. (1998) for a reliable estimation of relative palaeointensity (RPI). In addition, the spread of the mean grain sizes of the remanence carrying Ti-magnetites is small as the data cluster in the middle of the PSD range of the Day plot (Day *et al*. 1977; Fig. 6) demonstrates. The NRM intensities at a demagnetization level of 20 mT (J_{NRM20}) were normalized by the common concentration-dependent parameters κ_{LF}, J_{SIRM} and J_{ARM} at a demagnetization level of 20 mT (J_{ARM20}) (Fig. 13a). Comparing the different relative palaeointensity (RPI) estimates with the ratio of κ_{ARM}/κ_{LF} (being an indicator of magnetic grain size), it becomes evident that the records normalized by κ_{LF} and J_{SIRM} depend on variations in grain size (Fig. 13a), whereas the record normalized by J_{ARM20} does not. This is due to the fact that coarse grains contribute to κ_{LF} and J_{SIRM} but do not contribute significantly to J_{ARM} and J_{NRM}. Since the RPI record calculated with J_{ARM20} looks completely different to those obtained with κ_{LF} and J_{SIRM} as normalizers (Fig. 13a), additional calculations were made with J_{NRM} and J_{ARM} at higher AF demagnetization levels and using the slope method. The results are basically the same. Therefore, the record of J_{NRM20}/J_{ARM20}, as a representative for the different curves, was taken to be the most reliable indicator of variations in the intensity of the geomagnetic field. The RPI shows a linear decrease starting at 9 ka with little variability (Fig. 13a). Before 11 ka, variations in grain size also dominate the J_{NRM20}/J_{ARM20} records, which is not surprising. The transition from the Pleistocene into the Holocene is marked by pronounced changes in several climatic factors controlling sedimentation in the Tobago Basin, as reflected in the various sediment components (Fig. 8). This is linked to a transition from a sediment load with a variable concentration of both, fine- and coarse-grained Ti-magnetite, to a sediment composition with a nearly constant amount of fine-grained Ti-magnetite and a variable concentration of coarse-grained fraction. Biplots of κ_{ARM}/κ_{LF} (grain size) versus J_{NRM20}/J_{ARM20} and J_{NRM20}/J_{SIRM} (palaeointensity) confirm that, for most of the core, there is no linear relation between J_{NRM20}/J_{ARM20} and the grain size estimates (Fig. 13b).

In order to test the validity of the estimated RPIs by comparison to other records, a stacked J_{NRM20}/J_{ARM20} record for the Tobago Basin was created by numerical resampling of the J_{NRM20}/J_{ARM20} data sets from cores M35003-4 and M78/1_235-1 in 0.1 kyr steps and calculating the mean value for each time slice. The error range shown in Fig. 14 is given by the difference between the individual and the mean value for each time slice. The RPI record was then compared to the absolute intensity curves derived for this location from the CALS10K.1b (Korte *et al*. 2011) and pfm9k.1a (Nilsson *et al*. 2014) geomagnetic field models, as well as with data obtained from volcanic glass samples from the seafloor at the East Pacific Rise (EPR; Gee *et al*. 2000; Carlut *et al*. 2004), the Transmexican volcanic belt (Gonzalez *et al*. 1997), and from pottery from two sites in Mesoamerica (Morales *et al*. 2009; Alva-Valdivia *et al*. 2010). From nearby sited Guadeloupe two values determined on andesitic lavas are also available (Carlut & Quidelleur 2000) (Fig. 14).

The most striking difference between the RPI record from the Tobago Basin and the CALS10K.1b and pfm9k.1a models is the opposite trend during the last 7 kyr (Fig. 14) also opposing the geomagnetic dipole trend. While the sediment record shows a steady decrease until recent times, the models show an increase. The modelled intensity low at 6.6 ka however, is inexplicable, especially when the glass sample data are taken into account (Fig. 14). Admittedly, the models are only poorly constrained for this region and the studied time interval, lacking data from the northern half of South America (Korte *et al*. 2011), except for the last centuries where the models are constrained by data from direct field observation. Between 7 and 10 ka, the models and the Caribbean record show comparable trends. The RPI curve fits quite well to the EPR data (Gee *et al*. 2000; Carlut *et al*. 2004), except for the last 1 kyr, suggesting that the Tobago Basin record basically reflects a long-term trend of the geomagnetic intensity variations. Comparison with archaeomagnetic data from Guatemala and Chiapas (Alva-Valdivia *et al*. 2010) and the volcanic record from Mexico (Gonzalez *et al*. 1997) did not disconfirm these findings, but put a spotlight on a fundamental problem (Fig. 14). The scatter in the range of the virtual axial dipole moment (VADM) records from archaeomagnetic data from the same time slice is in general that large that it is not possible to use it reasonably neither for validation nor for calibration of sediment records. Other sedimentary RPI records from this region are not available, except for results of palaeomagnetic and magnetic susceptibility measurements of ODP cores from site 1002

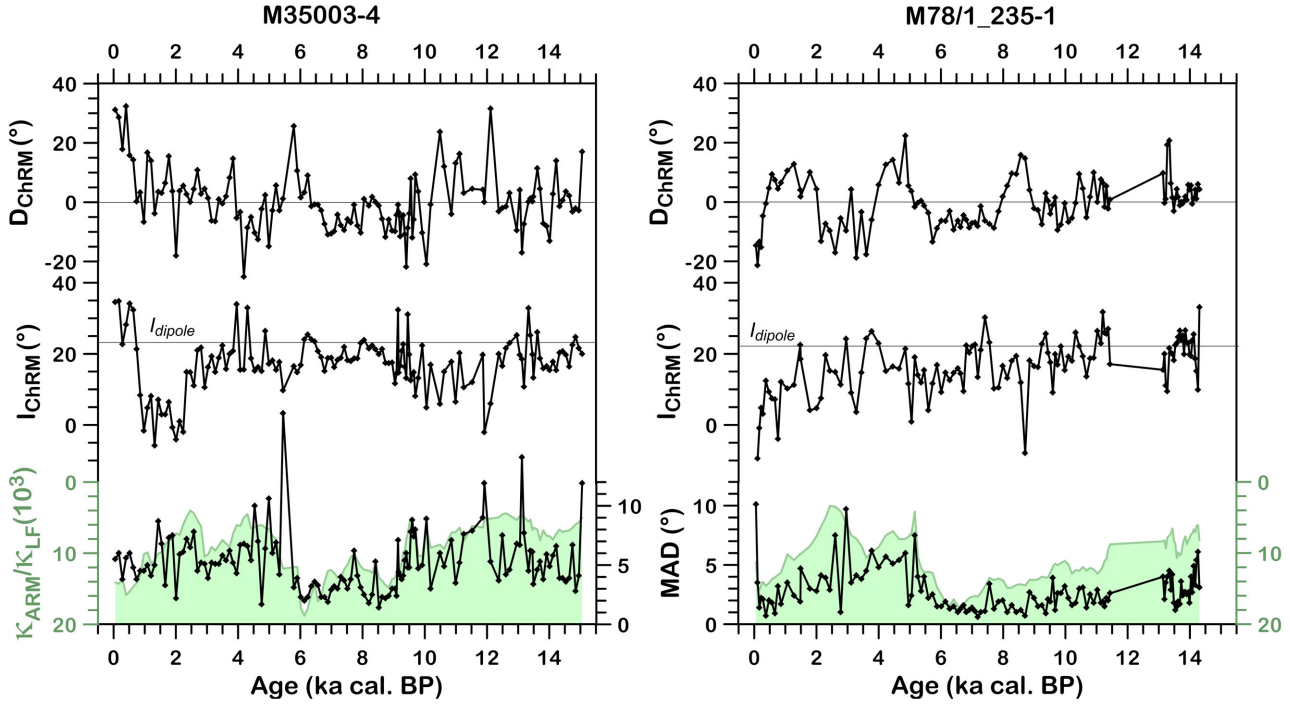

Figure 9. Left: ChRM inclination and declination curves for core M35003-4 and right: M78/1_235-1 versus age. Precision of the determined directions of the remanence vectors of each sample during demagnetization is quantified by the maximum angular deviation (MAD) values derived from the principal component analysis. Additionally are the κ_{ARM}/κ_{LF} records shown, highlighting the dependency of the MAD on the magnetic grain size.

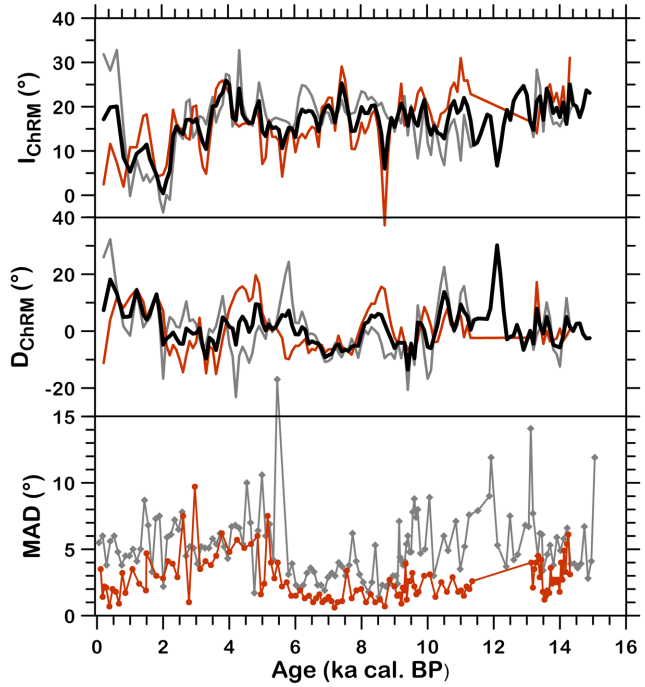

Figure 10. Direct comparison of the stacked inclination and declination records constructed for the Caribbean (black line) with the individual records, resampled in steps of 0.1 kyr from cores M35003-4 (grey line) and M78/1_235-1 (red line) and the MAD curves (see Fig. 9). For more details, see the text.

in the Cariaco Basin, 470 km to the southwest (Sigurdson *et al.* 1997) and different sites from Leg 155 on the Amazon Fan (Flood *et al.* 1995). Since the Cariaco Basin was anoxic during the last 14 kyr at least (Haug *et al.* 2001) the magnetic fraction within the sediments is severely affected by diagenesis. Thus, no useful records of geomagnetic field variations could be expected here. In front of the Amazon Fan, the sedimentation rate drops distinctly from >90 to 7 cm kyr^{-1} at around 10 ka, a consequence of the increasing sea level after the end of the last glacial (Maslin *et al.* 2000). In addition, the available NRM/ARM record for ODP Hole 932A did not cover the time interval in question (Cisowski & Hall 1997). Further to the north, palaeomagnetic investigations were carried out on a number of sediment cores from the Blake/Bahama Outer Ridge and the Bermuda Rise (Schwartz *et al.* 1998; Lund *et al.* 2005; Lund *et al.* 2006; Channell et al. 2012). But, most of these records did lack the Holocene as well, or the resolution is too low for comparison.

On a global scale, there are several RPI records from the Atlantic and the Pacific that show a decreasing trend similar to the one observed in the Carribean (Fig. 15). The high-resolution record for ODP Site 1202 (Richter *et al.* 2006) for example, displays a decrease in intensity for the last 5 kyr (Fig. 15). Two identical records from sediments off Cape Ghir, North West Africa (Bleil & Dillon 2008) show also a decrease for the last 4 kyr. The South Atlantic Palaeointensity Stack (SAPIS) comprises two records with decreasing trends for the last 7 kyr, cores 21PC-02 and ODP Site 1089 (Stoner *et al.* 2002). The best fit is given between the Tobago Basin and the MD95-2024 records (Stoner *et al.* 2000), both showing a long-term decrease for the last 10 kyr (Fig. 15). Marine RPI records from the North Atlantic east of 30°W and the St. Lawrence Estuary record however, show a different behaviour, resembling the Fennoscandian relative palaeointensity stack (FENNORPIS) (Snowball *et al.* 2007) and the archaeomagnetic record for Bulgaria (Kovacheva *et al.* 2014), representatives of Europe as a whole, with its well-defined increase in palaeointensity between 6 and 2.5 ka, and a steady decrease since 2 ka until recent times (Fig. 15). The other records shown in Fig. 15, chosen either for their geographical position, or, in case of regional abundance, their

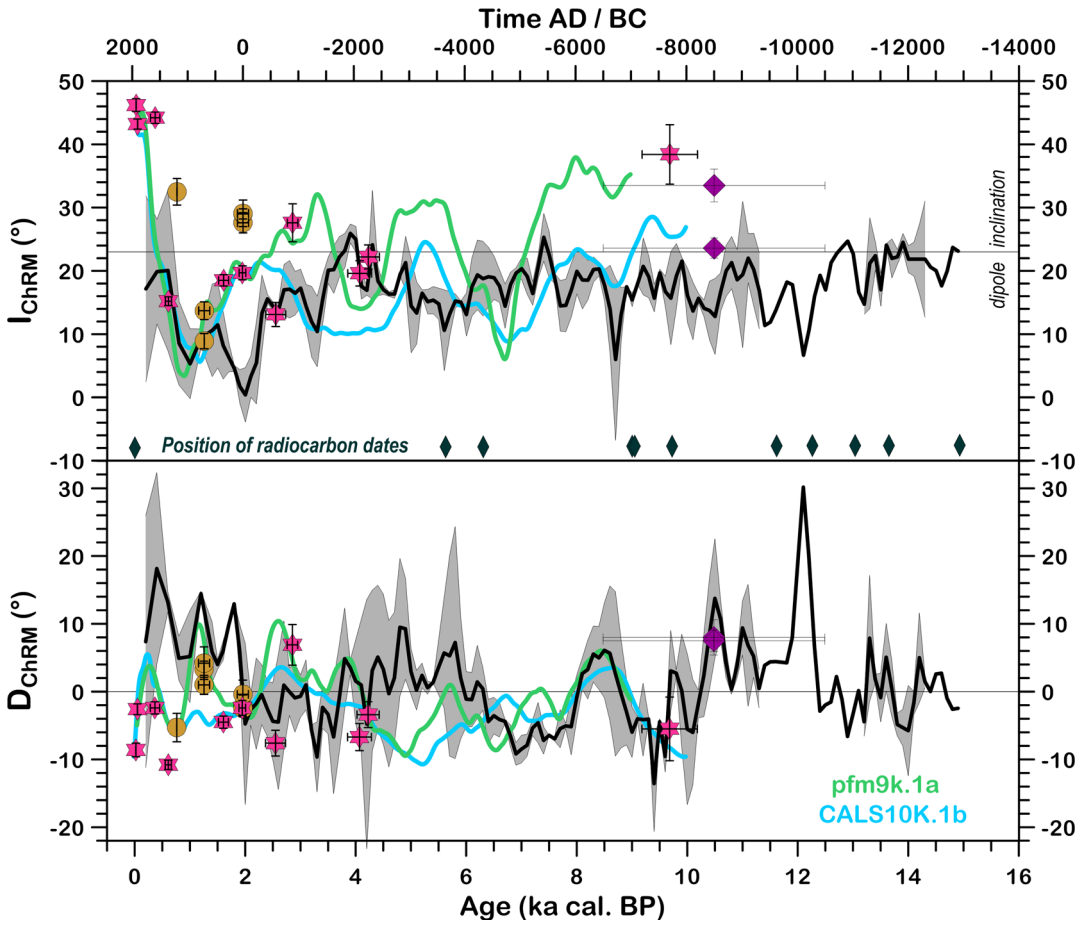

Figure 11. Comparison of the stacked ChRM inclination and declination records for Tobago Basin (black lines) with other data and modelled curves for the study area (see also Fig. 1): CALS10K.1b (Korte *et al*. 2011); pfm9k.1a (Nilsson *et al*. 2014): pink stars—volcanic data from Montagne Pelée (Genevey *et al*. 2002; Tanty *et al*. 2015), purple diamonds—La Guadeloupe Island (Carlut & Quidelleur 2000) and golden filled circles—archaeomagnetic data from El Salvador (Eighmy & Sternberg 1990). Error bars are shown when available. The grey-shaded area denotes the difference between the inclination and declination curves for cores M35003-4 and M78/1_235-1 and the stacked curve.

sedimentation rate, display a wide range of variability with little regional coherence. This indicates that either the regional variability of the non-dipole component of the Earth's magnetic field vector is higher than expected, or that some of the RPI records are still influenced by sediment composition. But, the latter is no explanation for the observed trend in the cores from the Caribbean presented here, since this trend is not reflected in any of the rock magnetic parameters (Fig. 7). It would have been helpful for the discussion if the Caribbean record and the other short records were not only covering the last 15 ka but instead 50 ka at least, thus allowing for a better assessment of the long-term trend and abrupt changes. Especially in the time interval 10–15 ka, the transition from the Pleistocene into the Holocene, the sedimentary records are frequently affected by the climatically induced variability in sediment load, composition, productivity and conditions at the sediment/water interface.

One main aspect of this study was to find evidence whether the SAA, a westward moving region of low intensity during historical times (Mandea *et al*. 2007; Hartmann & Pacca 2009; Pavón-Carrasco & De Santis 2016) persisted or whether it is a recurring feature already since the early Holocene. The RPI records presented here did not allow for an interpretation in terms of regional differences in absolute intensity. This must be done by including these new data sets into the global models. However, the records from the Caribbean in combination with those from Cape Ghir (Bleil & Dillon 2008), Laguna Potrok Aike (Lisé-Pronovost *et al*. 2013) and SAPIS (Stoner *et al*. 2002), all located at the outer border of the SAA area, as it is defined today, show coherently a distinctively earlier decline in geomagnetic field intensity than in Europe and especially at it's northernmost locations (Fig. 15). A second region with similar behaviour is the West Pacific including records from Lake Biwa, Japan (Hayashida *et al*. 2007), ODP hole 1202B (Richter *et al*. 2006) and the Ontong-Java Plateau, core e113p (Tauxe & Wu 1990; Fig. 15). Nowadays, this region is also characterized by a low in total intensity as visible in the International Geomagnetic Reference Field for the last decades (http://www.ngdc.noaa.gov/IAGA/vmod/igrf.html, last accessed 11 January 2017). Unfortunately, both regions comprise vast areas of the ocean that are in general not well covered by high-resolution sediment records, especially for the Holocene. This is due to a number of reasons including disturbance of the top sediment during coring, low sedimentation rates in the middle of wide marine basins and the development of new sediment deposition patterns on the continent shelves as a consequence of the global sea level rise during the last 14 kyr. Regardless the confirmation by ongoing investigations on sediments from both sides of the South Atlantic, the differences between the observed RPI patterns and model or reference data indicate larger contributions by the non-dipole field compounds to the

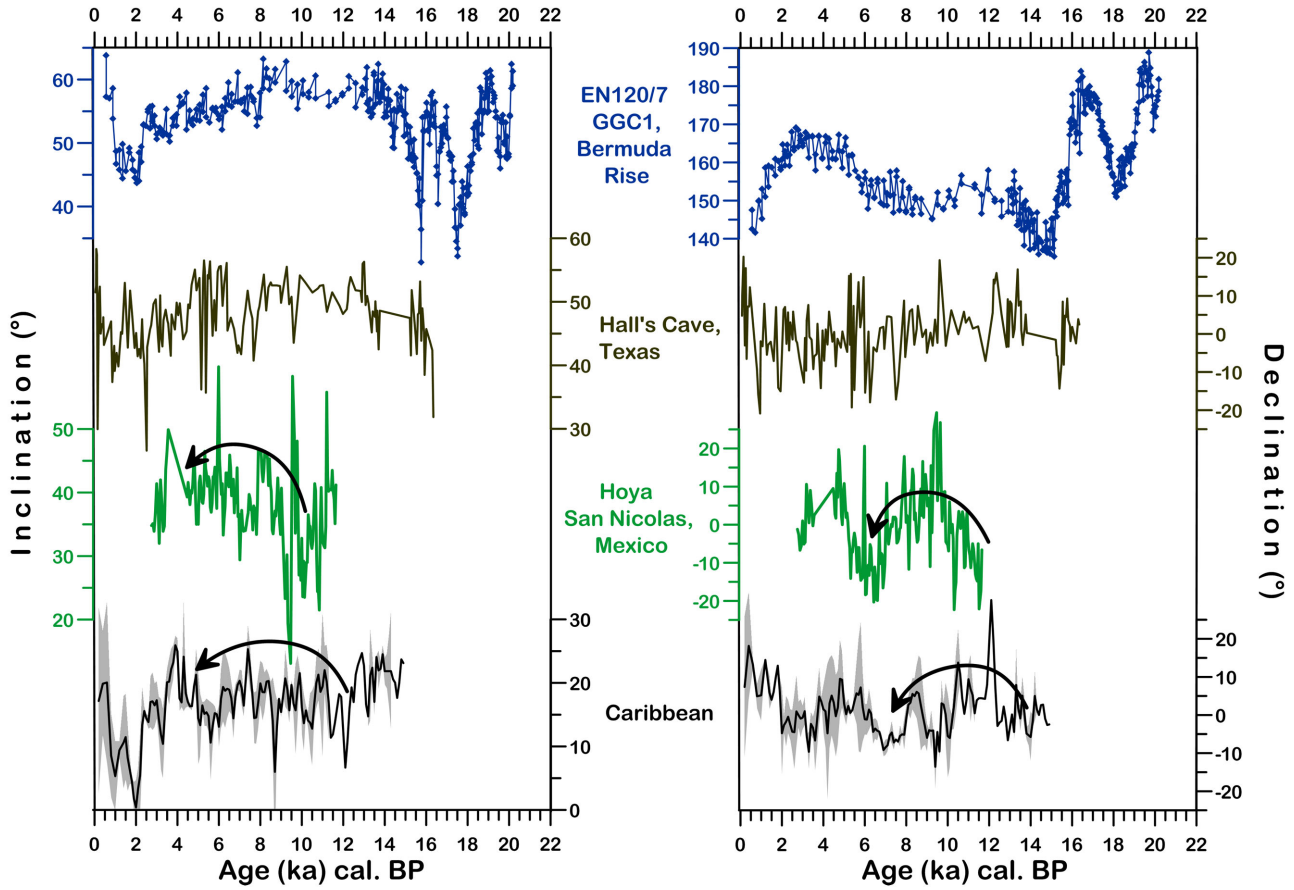

Figure 12. Comparison of the new Caribbean PSV record with other records on a wider regional scale: core EN120/7 GGC1 from Bermuda Rise (Lund & Keigwin 1994), Hall's Cave, Texas (Bourne *et al*. 2016) and Hoya de San Nicolas, Mexico (Chaparro *et al*. 2008). The four locations denote the corners of a slightly irregular quadrangle, with the Bermuda Rise core (33.67°N, 57.62°W) being from a similar longitude as the Caribbean core locations (~11.8°N, 61.1°W) and from a similar latitude as Hall's Cave (30.13°N, 99.54°W). The latter is also from a similar longitude as Hoya San Nicolas, Mexico (20.39°N, 101.26°W).

field geometry throughout the studied time interval in the Caribbean area.

CONCLUSIONS

The palaeomagnetic investigations carried out on cores M35003-4 and M78/1_235-1 from Tobago Basin yielded the first set of high-resolution PSV records for the Eastern Caribbean for the last 15 kyr. Rock magnetic investigations in combination with results of former sedimentological and geochemical studies revealed that there are at least two magnetic mineral fractions with different origins contained in the sediment: Ti-magnetites in the PSD range originating from the sediment load of the Amazon River and transported north by the North Brazil and the Guyana Current are the main carriers of the magnetic signal. Coarser-grained magnetic material, probably originating from the nearby Orinoco River causes the observed variations in magnetic concentration, grain size and coercivity, thus masking the presence of the fine-grained fraction in most rock magnetic parameters. Since the high variability in the coarse-grained magnetic fraction is not reflected in the RPI estimates calculated with J_{ARM20} as normalization parameter, the J_{NRM20}/J_{ARM20} records are supposed to be a reliable representation of geomagnetic intensity variations. In global context, the stacked RPI record for the Caribbean corresponds to records from the southern Atlantic and low-latitude Pacific sites, displaying a decreasing trend for the last 9 kyr. A more clear interpretation of the records in terms of non-dipole field behaviour during the Holocene is not yet feasible until more high-quality and high-resolution RPI records from low (northern) latitudes and the southern hemisphere, especially from the Atlantic sector become available. Nevertheless, the new data from the Caribbean are a valuable contribution to the database needed for the development of precise global geomagnetic field models.

ACKNOWLEDGEMENTS

The authors would like to thank V. Bender and J. Schönfeld for providing access to the sediment cores at MARUM, Bremen and GEOMAR, Kiel, respectively. A. Vink and M. Hüls are kindly acknowledged for providing their data of core M35003-4. All the holders of the geomagnetic reference data are thanked for providing their data sets either on personal request or make them accessible to the public via databases like the GEOMAGIA and PANGAEA or as publication supplements. Two anonymous reviewers are acknowledged for their comments on a former version of this paper. This study was funded by the German Research Foundation (DFG), grant no. KO 2870/4-1, within the scope of the priority programme (SPP) 1488 'Planetary Magnetism'.

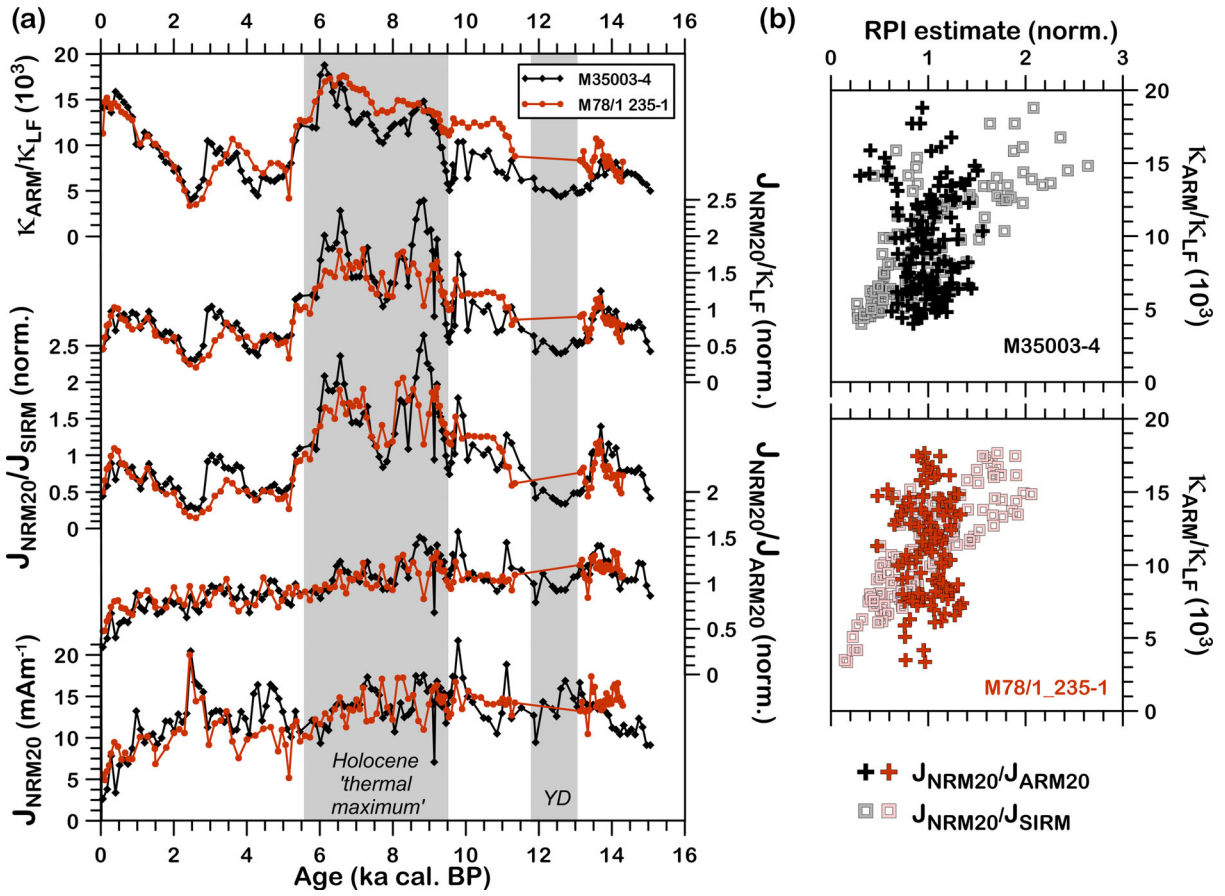

Figure 13. (a) Time-series of from bottom to top NRM intensities after demagnetization at a level of 20 mT (J_{NRM20}), relative palaeointensities estimated by dividing J_{NRM20} by different parameters (κ_{LF}, J_{SIRM} and J_{ARM20}) and then normalizing to the mean value, completed by the grain-size dependent parameter κ_{ARM}/κ_{LF} versus age. (b) Biplots of estimated relative palaeointensities versus grain size estimate (κ_{ARM}/κ_{LF}). Palaeointensities are calculated by normalizing J_{NRM20} by J_{SIRM} and J_{ARM20}, respectively. Only the ARM-based palaeointensity estimate is independent of grain size variations in both cores.

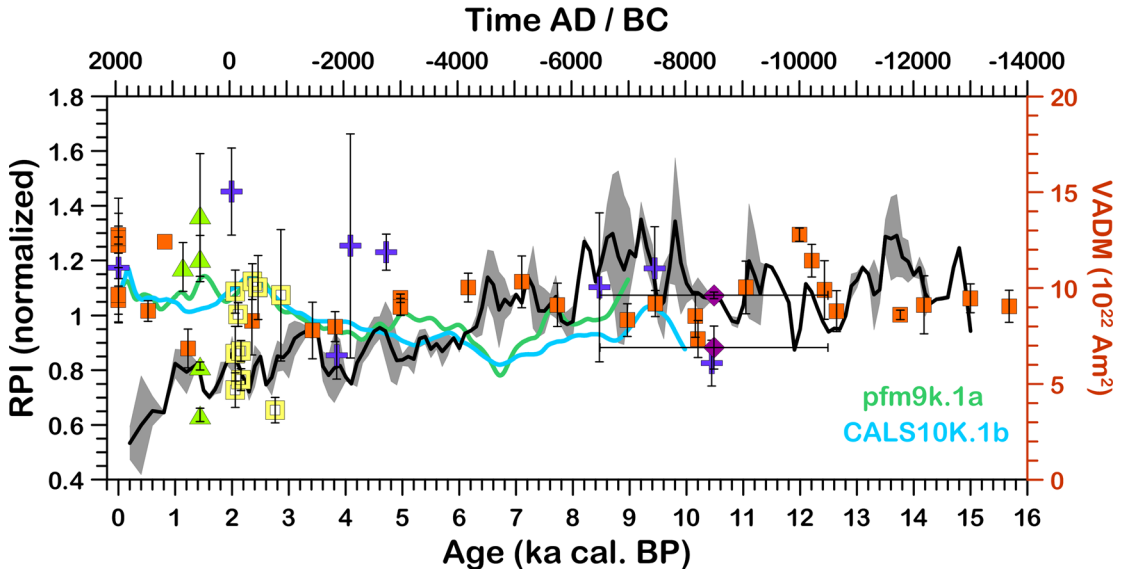

Figure 14. Comparison of stacked relative palaeointensity (RPI) record from Tobago Basin with modelled virtual axial dipole moment (VADM) curves for this location (CALS10K.1b; Korte *et al*. 2011 and pfm9k.1a; Nilsson *et al*. 2014), and volcanic and archaeomagnetic data from the region (compare Fig. 1): orange squares—volcanic glass samples from the East Pacific Rise (Gee *et al*. 2000; Carlut *et al*. 2004); purple diamonds—lava flow La Guadeloupe Island (Carlut & Quidelleur 2000); blue crosses—Transmexican volcanic belt (Gonzalez *et al*. 1997); yellow open squares—Guatemalan pottery (Alva-Valdivia *et al*. 2010) and green triangles—Chiapas pottery (Morales *et al*. 2009). The difference between the J_{NRM20}/J_{ARM20} records for cores M35003-4 and M78/1_235-1 and the stacked RPI record is indicated by the grey-shaded area.

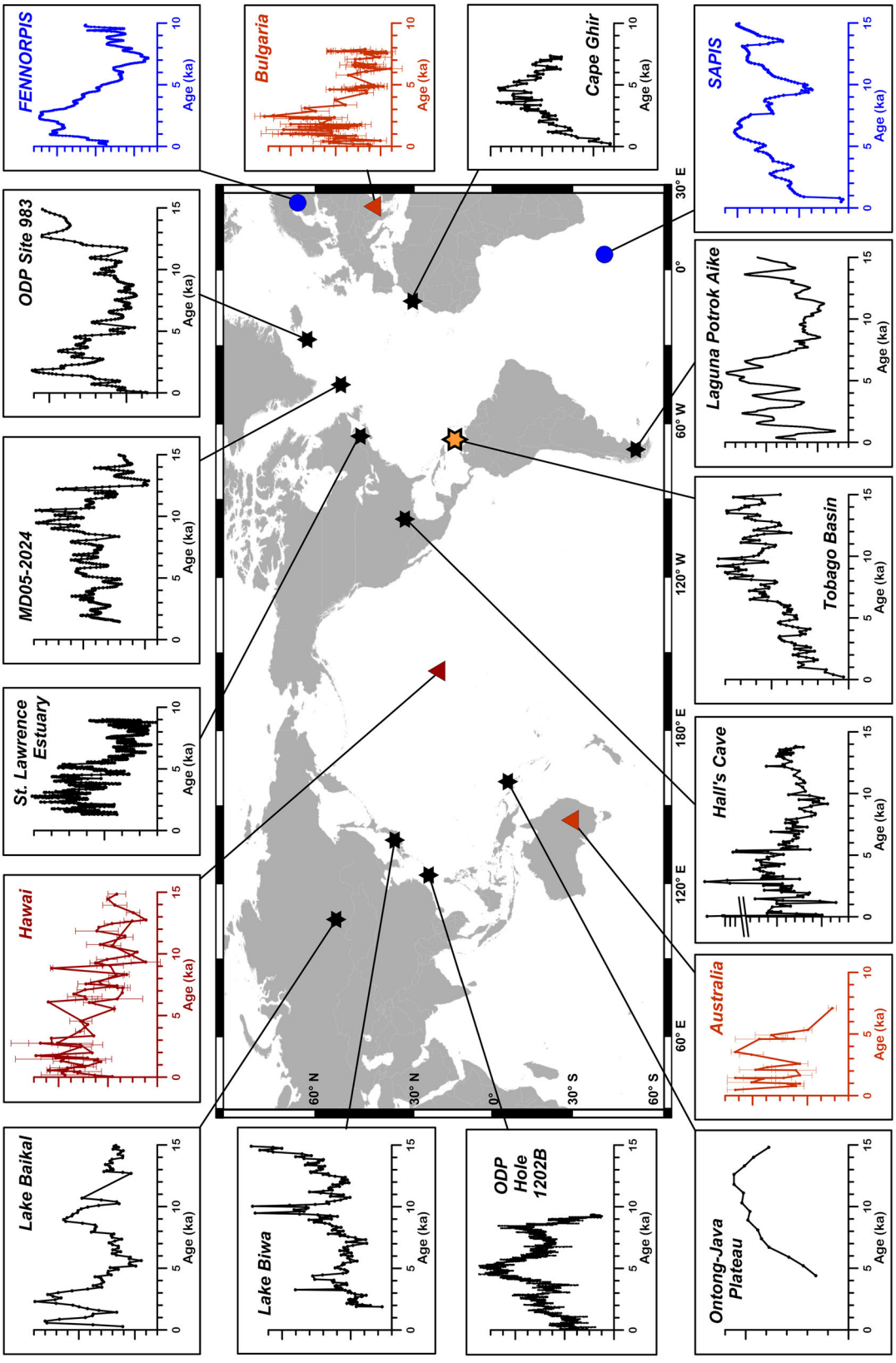

Figure 15. Compilation of (relative) palaeointensity records for the last 15 kyr and their spatial distribution on a global map. Absolute intensity records from lavas (dark red): Hawai (Laj *et al.* 2002; Teanby *et al.* 2002), and archaeomagnetic material (red): Bulgaria (Kovacheva *et al.* 2014) and Australia (Barbetti 1983). Stacked relative palaeointensity (RPI) records (blue): Fennoscandian relative palaeointensity stack (FENNORPIS) (Snowball *et al.* 2007) and the South Atlantic Palaeointensity Stack (SAPIS; Stoner *et al.* 2002). RPI records from single sites (black): Cape Ghir, NW Africa, continental margin, core GeoB 6007-2 (Bleil & Dillon 2008); Laguna Potrok Aike, Argentina (Lisé-Pronovost *et al.* 2013); Tobago Basin (this study); Hall's Cave, Texas, USA (Bourne *et al.* 2016); Ontong-Java Plateau, core e113p (Tauxe & Wu 1990); ODP hole 1202B, West Pacific (Richter *et al.* 2006); Lake Biwa, Japan (Hayashida *et al.* 2007); Lake Baikal, Siberia (Peck *et al.* 1996), St. Lawrence Estuary, Canada (St-Onge *et al.* 2003) and the North Atlantic: MD05-2024 (Stoner *et al.* 2000) and ODP site 983 (Channell *et al.* 1997). In order to enhance the clarity of the figure, the *Y*-axes were plotted without titles and labels. For the absolute intensity records (Hawai, Bulgaria and Australia), the spacing between major ticks is equal to 20 μT. Except for Lake Baikal (scaled virtual axial dipole moment, VADM), Lake Biwa (NRM/ARM) and Texas (intensity) different types of normalized intensity values are plotted on the *Y*-axis of all RPI records with the major ticks denoting 0.5 (arb. units). For detailed information, the reader is referred to the referenced publications. A different scaling of the *Y*-axes was chosen in order to highlight the overall trends in the (R)PI curves rather than to compare absolute numbers.

REFERENCES

Alva-Valdivia, L.M., Morales, J., Goguitchaichvilli, A., Hatch, M.P.d., Hernandes-Bernal, M.S. & Mariano-Matías, F., 2010. Absolute geomagnetic intensity data from preclassic Guatemalan pottery, *Phys. Earth planet. Inter.,* **180,** 41–51.

Bahr, A., 2012a. Color data of sediment core M78/1_235-1, PANGAEA, doi:10.1594/PANGAEA.788740.

Bahr, A., 2012b. Magnetic susceptibility of sediment core M78/1_235-1, PANGAEA, doi:10.1594/PANGAEA.788760.

Bahr, A. *et al.*, 2013. Comparison of Ba/Ca and $d^{18}O_{WATER}$ as freshwater proxies: a multi-species core-top study on planktonic foraminifera from the vicinity of the Orinoco River mouth, *Earth planet. Sci. Lett.,* **383,** 45–57.

Barbetti, M., 1983. Archaeomagnetic results from Australia, in *Geomagnetism of Baked Clays and Recent Sediments*, pp. 173–175, eds Creer, K.M., Tucholka, P. & Barton, C.E., Elsevier.

Bleil, U. & Dillon, M., 2008. Holocene earth's magnetic field variations recorded in marine sediments of the NW African continental margin, *Stud. Geophys. Geod.,* **52,** 133–155.

Bourne, M.D., Feinberg, J.M., Stafford Jr., T.W., Waters, M.R., Lundelius Jr., E. & Forman, S.L., 2016. High-intensity geomagnetic field 'spike' observed at *ca*. 3000 cal BP in Texas, USA, *Earth planet. Sci. Lett.,* **442,** 80–92.

Bouysse, P. & Mascle, A., 1994. Sedimentary basins and petroleum plays around the French Antilles, in *Hydrocarbon and Petroleum Geology of France,* Vol. 4, pp. 431–443, ed. Mascle, A., Springer.

Carlut, J., Cormier, M.-H., Kent, D.V., Donnelly, K.E. & Langmuir, C.H., 2004. Timing of volcanism along the northern East Pacific Rise based on paleointensity experiments on basaltic glasses, *J. geophys. Res.,* **109,** B04104, doi:10.1029/2003JB002672.

Carlut, J. & Quidelleur, X., 2000. Absolute paleointensities recorded during the Brunhes chron at La Guadeloupe Island, *Phys. Earth planet. Inter.,* **120,** 255–269.

Channell, J.E.T., Hodell, D.A. & Lehman, B., 1997. Relative geomagnetic paleointensity and $d^{18}O$ at ODP site 983 (Gardar Drift, North Atlantic) since 350 ka, *Earth planet. Sci. Lett.,* **153,** 103–118.

Channell, J.E.T., Hodell, D.A. & Curtis, J.H., 2012. ODP Site 1063 (Bermuda Rise) revisited: oxygen isotopes, excursions and paleointensity in the Brunhes Chron, *Geochem. Geophys. Geosyst.,* **13,** Q02001, doi:10.1029/2011GC003897.

Chaparro, M.A.E., Böhnel, H.N., Byrne, R., Nowaczyk, N.R., Molina-Garza, R.S., Park, K. & Negendank, J.F.W., 2008. Paleomagnetic secular variation and rock-magnetic studies of Holocene sediments from a maar lake (Hoya de San Nicolas) in Central Mexico, *Geophys. J. Int.,* **175,** 462–476.

Chérubin, L.M. & Richardson, P.L., 2007. Caribbean current variability and the influence of the Amazon and the Orinoco freshwater plumes, *Deep-Sea Res. I. Oceanogr. Res. Pap.,* **54,** 1451–1473.

Cisowski, S.M. & Hall, F.R., 1997. An examination of the paleointensity record and geomagnetic excursions recorded in LEG 155 cores, in *Proceedings of the Ocean Drilling Program, Scientific Results,* Vol. 155, pp. 231–243, Ocean Drilling Program, College Station, TX.

Damuth, J.E., 1977. Late Quaternary sedimentation in the western equatorial Atlantic, *Bull. geol. Soc. Am.,* **88,** 695–710.

Day, R., Fuller, M. & Schmidt, V.A., 1977. Hysteresis properties of titanomagnetites: grain size and compositional dependence, *Phys. Earth planet. Inter.,* **13,** 260–267.

Dunlop, D.J., 2002. Theory and application of the Day plot (M_{rs}/M_s versus H_{cr}/H_c) 1. Theoretical curves and tests using titanomagnetite data, *J. geophys. Res.,* **107**(B3), 2056, doi:10.1029/2001JB000486.

Eighmy, J.L. & Sternberg, R., 1990. *Archaeomagnetic Dating,* University of Arizona Press, 446 pp.

Flood, R.D. *et al.*, 1995. Amazon fan sites 930–946, in *Proceedings of the ODP Initial Reports*, Vol. 155, College Station, TX, 702 pp..

Frank, U. & Nowaczyk, N.R., 2008. Mineral magnetic properties of artificial samples systematically mixed from haematite and magnetite, *Geophys. J. Int.,* **175,** 449–461.

Gee, J.S., Cande, S.C., Hildebrand, J.A., Donnelly, K. & Parker, R.L., 2000. Geomagnetic intensity variations over the past 780 kyr obtained from near-seafloor magnetic anomalies, *Nature,* **408,** 827–832.

Genevey, A., Gallet, Y. & Boudon, G., 2002. Secular variation study from non-welded pyroclastic depoits from Montagne Pelée volcano (West Indies), *Earth planet. Sci. Lett.,* **201,** 369–382.

Gonzalez, S., Sherwooh, G., Böhnel, H. & Schnepp, E., 1997. Paleosecular variation in Central Mexico over the last 30000 years: the record from lava, *Geophys. J. Int.,* **130,** 201–2019.

Govin, A., Chiessi, C.M., Zabel, M., Sawakuchi, A.O., Heslop, D., Hörner, T., Zhang, Y. & Multza, S., 2014. Terrigenous input off northern South America driven by changes in Amazonian climate and the North Brazil Current retroflection during the past 250 ka, *Clim. Past.,* **10,** 843–862.

Hartmann, G.A. & Pacca, I.G. 2009. Time evolution of the South Atlantic Magnetic anomaly. *Ann. Brazil. Acad. Sci.,* **81,** 243–255.

Haug, G.H., Hughen, K.A., Sigman, D.M., Peterson, L.C. & Röhl, U., 2001. Southward migration of the intertropical convergence zone through the Holocene, *Science,* **293,** 1304–1308.

Hayashida, A., Ali, M., Kuniko, Y., Kitagawa, H., Torii, M. & Takemura, K., 2007. Environmental magnetic record and paleosecular variation data for the last 40 kyrs from the Lake Biwa sediments, Central Japan, *Earth Planets Space,* **59,** 807–814.

Hemleben, C., Zahn, R. & Meischner, D., eds, 1998. Karibik 1996—Cruise No. M35/1 (April 18–June 3, 1996), in *METEOR_Berichte 98-3*, Leitstelle METEOR, Institut fiir Meereskunde der Universitat Hamburg, 208 pp.

Hoffmann, J., Bahr, A., Voigt, S., Schönfeld, J., Nürnberg, D. & Rethemayer, J., 2014a. Disentangling abrupt deglacial hydrological changes in northern South America: insolation versus oceanic forcing, *Geology,* **42,** 579–582

Hoffmann, J., Bahr, A., Voigt, S., Schönfeld, J., Nürnberg, D. & Rethemayer, J., 2014b. Age determination and stable isotope records of sediment core M78/1_235-1. doi:10.1594/PANGAEA.833373.

Hüls, M., 1999. Total organic carbon and calcium carbonate of sediment core M35003-4, PANGAEA, doi:10.1594/PANGAEA.55753.

Hüls, M. & Zahn, R., 2000. Millennial-scale Sea surface temperature variability in the western tropical North Atlantic from planktonic foraminiferal census counts, *Paleoceanography,* **15,** 659–678.

Johns, W.E., Townsend, T.L., Fratantoni, D.M. & Wilson, W.D., 2002. On the Atlantic inflow to the Caribbean Sea, *Deep-Sea Res. I. Oceanogr. Res. Pap.,* **49,** 211–243.

Kirschvink, J.L., 1980. The least-squares line and plane and the analysis of palaeomagnetic data, *Geophys. J. R. astr. Soc.,* **62,** 699–718.

Korte, M., Constable, C., Donadini, F. & Holme, R., 2011. Reconstructing the Holocene geomagnetic field, *Earth planet. Sci. Lett.,* **312,** 497–505.

Korte, M., Donadini, F. & Constable, C.G., 2009. Geomagnetic field for 0–3 ka: 2. A new series of time-varying global models, *Geochem. Geophys. Geosyst.,* **10**, Q06008, doi:10.1029/2008GC002297.

Kovacheva, M., Kostadinova-Avramova, M., Jordanova, N., Lanos, P. & Boyadziev, Y., 2014. Extended and revised archeomagnetic database and secular variation curves for Bulgaria for the last eight millenia, *Phys. Earth planet. Inter.,* **236,** 79–94.

Laj, C., Kissel, C., Scao, V., Beer, J., Thomas, D.M., Guillou, H., Muscheler, R. & Wagner, G., 2002. Geomagnetic intensity and inclination variations at Hawaii for the past 98 kyr from SOH-4 (Big Island): a new study and a comparison with existing contemporary data, *Phys. Earth planet. Inter.,* **129,** 205–243.

Lisé-Pronovost, A. *et al.*, 2013. High-resolution paleomagnetic secular variations and relative paleointensity since the Late Pleistocene in southern America, *Quat. Sci. Rev.,* **71,** 91–108.

Lund, S.P. & Keigwin, L., 1994. Measurements of the degree of smoothing in sediment paleomagnetic secular variation records: an example from late Quaternary deep-sea sediments of the Bermuda Rise, western North Atlantic Ocean, *Earth planet. Sci. Lett.,* **122,** 317–330.

Lund, S., Stoner, J.S., Channell, J.E.T. & Acton, G., 2006. A summary of Brunhes paleomagnetic field variability recorded in Ocean Drilling Program cores, *Phys. Earth planet. Inter.,* **156,** 194–204.

Lund, S.P., Schwartz, M., Keigwin, L. & Johnson, T., 2005. Deep-sea sediment records of the Laschamp geomagnetic field excursion

(∼41 000 calendar years before present), *J. geophys. Res.,* **110,** doi:10.1029/2003JB002943.

Mandea, M., Korte, M., Mozzoni, D. & Kotzé, P., 2007. The magnetic field changing over the southern African continent: a unique behaviour, *South Afr. J. Geol.,* **110,** 193–202.

Maslin, M.A. & Burns, S.J., 2000. Reconstruction of the Amazon Basin effective moisture availability over the past 14 000 years, *Science,* **290,** 2285–2287.

Maslin, M.A. *et al.*, 2000. Palaeoreconstruction of the Amazon River freshwater and sediment discharge using sediments recovered at Site 942 on the Amazon Fan, *J. Quat. Sci.,* **15,** 419–434.

Morales, J., Goguitchaichvili, A., Acosta, G., Gonzáles-Moran, T., Alva-Valdivia, L., Robles-Camacho, J. & Hernández-Bernal, M.d.S., 2009. Magnetic properties and archeointensity determination on Precolumbian pottery from Chiapas, Mesoamerica, *Earth Planets Space,* **61,** 83–91.

Nilsson, A., Holme, R., Korte, M., Suttie, N. & Hill, M., 2014. Reconstructing Holocene geomagnetic field variation: new methods, models and implications, *Geophys. J. Int.,* **198,** 229–248.

Nowaczyk, N.R., 2011. Dissolution of titanomagnetite and sulphidization in sediments from Lake Kinneret, Israel, *Geophys. J. Int.,* **187,** 34–44.

Opdyke, N.D. & Channell, J.E.T., 1996. *Magnetic Stratigraphy*, Academic Press, 346 pp.

Parry, L.G., 1980. Shape-related factors in the magnetization of immobilized magnetite particles, *Phys. Earth planet. Inter.,* **22,** 144–154.

Parry, L.G., 1982. Magnetization of immobilized particle dispersion with two distinct particle sizes, *Phys. Earth. Planet. Int.,* **28,** 230–241.

Pavón-Carrasco, F.J. & De Santis, A., 2016. The South Atlantic anomaly: the key for a possible geomagnetic reversal, *Front. Earth Sci.,* **4,** doi:10.3389/feart.2016.00040.

Peck, J.A., King, J.W., Colman, S.M. & Kravchinsky, V.A., 1996. An 84-kyr paleomagnetic record from the sediments of Lake Baikal, Siberia, *J. geophys. Res.,* **101,** 11 365–11 385.

Richter, C., Venuti, A., Verosub, K.L. & Wei, K.-Y., 2006. Variations of the geomagnetic field during the Holocene: relative paleointensity and inclination record from the West Pacific (ODP Hole 1202B), *Phys. Earth planet. Inter.,* **156,** 179–193.

Roberts, A.P., Cui, Y. & Verosub, K.L., 1995. Wasp-waisted hysteresis loops: mineral magnetic characteristics and discrimination of components in mixed magnetic systems, *J. geophys. Res.,* **100,** 17 909–17 924.

Roud, S.C., 2014. Magnetic mineral inventory of late Quaternary sediments from the tropical Atlantic Off North Brazil: indicator for paleoenvironmental conditions and early diagenesis, *Master Masterarbeit,* Fachbereich Geowissenschaften, Universität Bremen, 62 pp.

Rühlemann, C., Mulitza, S., Müller, P.J., Wefer, G. & Zahn, R., 1999. Warming of the tropical Atlantic Ocean and slowdown of thermohaline circulation during the last deglaciation, *Nature,* **402,** 511–514.

Rühlemann, C., Mulitza, S., Müller, P.J., Wefer, G. & Zahn, R., 2006. (Table 1) Age determination of sediment core M35003-4, doi:10.1594/PANGAEA.438798.

Schönfeld, J. *et al.*, 2011. Surface and Intermediate Water hydrography, planktonic and benthic biota in the Caribbean Sea - Climate, Bio and Geosphere linkages (OPOKA) – Cruise No. M78/1 (February 22–March 28, 2009) – Colón (Panama) – Port of Spain (Trinidad and Tobago), in *METEOR-Berichte,* M78/1, 40 pp., DFG-Senatskommission für Ozeanographie, doi:10.2312/cr_m78_1.

Schwartz, M., Lund, S.P. & Johnson, T.C., 1998. Geomagnetic field intensity from 71 to 12 ka as recorded in deep-sea sediments of the Blake Outer Ridge, North Atlantic Ocean, *J. geophys. Res.,* **103,** 30 407–430 416.

Sigurdson, H., Leckie, R.M. & Acton, G.D. & Shipborad Scientific Party, 1997. Site 1002, in *Proceedings of the ODP Initial Reports*, Vol. 165, pp. 359–373, College Station, TX.

Snowball, I., Zillén, L., Ojala, A., Saarinen, T. & Sandgren, P., 2007. FENNOSTACK and FENNORPIS: Varve dated Holocene paleomagnetic secular variation and relative paleointensity stacks for Fennoscandia, *Earth planet. Sci. Lett.,* **255,** 106–116.

Stoner, J.S., Channel, J.E.T., Hillaire-Marcel, C. & Kissel, C., 2000. Geomagnetic paleointensity and environmental record from Labrador Sea core MD95-2024: global marine sediment and ice core chronostratigraphy for the last 110 kyr, *Earth planet. Sci. Lett.,* **183,** 161–177.

Stoner, J.S., Laj, C., Channell, J.E.T. & Kissel, C., 2002. South Atlantic and North Atlantic geomagnetic paleointensity stacks (0–80 ka): implications for inter-hemispheric correlation, *Quat. Sci. Rev.,* **21,** 1141–1151.

St-Onge, G., Stoner, J.S. & Hillaire-Marcel, C., 2003. Holocene paleomagnetic records from the St. Lawrence Estuary, eastern Canada: centennial- to millennial-scale geomagnetic modulation of cosmogenic isotopes, *Earth planet. Sci. Lett.,* **209,** 113–130.

Stuiver, M. & Reimer, P.J., 1993. Extended ^{14}C data base and revised Calib 3.0 ^{14}C age calibration program, *Radiocarbon,* **35,** 215–230.

Stuiver, M., Reimer, P.J. & Reimer, R., 2013. CALIB radiocarbon calibration Version 7.0. Available at: http://calib.qub.ac.uk/calib/, last accessed 11 January 2017.

Tanty, C., Carlut, J., Valet, J.-P. & Germa, A., 2015. Paleosecular variation recorded by 9 ka to 2.5-Ma-old lavas from Martinique Island: new evidence for the La Palma aborted reversal ∼617 ka ago, *Geophys. J. Int.,* **200,** 915–932.

Tauxe, L. & Wu, G., 1990. Normalized remanence in sediments of the Western Equatorial Pacific: relative paleointensity of the geomagnetic field, *J. geophys. Res.,* **95,** 12 337–12 350.

Teanby, N., Laj, C., Gubbins, D. & Pringle, M., 2002. A detailed palaeointensity and inclination record from drill core SOH1 on Hawaii, *Phys. Earth planet. Inter.,* **131,** 101–140.

Vink, A., Rühlemann, C., Zonnefeld, K.A.F., Mulitza, S., Hüls, M. & Willems, H., 2001. Shifts in the position of the North Equatorial Current and rapid productiviry changes in the western Tropical Atlantic during the last glacial, *Paleoceanography,* **16,** 479–490.